1-1-2000

Scene-based nonuniformity correction with video sequences and registration

Russell C. Hardie
University of Dayton

Majeed M. Hayat
Marquette University, majeed.hayat@marquette.edu

Earnest Armstrong
U.S. Air Force Research Laboratory

Brian Yasuda
U.S. Air Force Research Laboratory

Accepted version. *Applied Optics*, Vol. 39, No. 8 (2000): 1241-1250. DOI.

Applied Optics, Vol. 39, No. 8 (2000): 1241-1250. DOI.

Scene-based nonuniformity correction with video sequences and registration

Russell C. Hardie
University of Dayton
Majeed M. Hayat
University of Dayton
Earnest Armstrong
The Air Force Research Labs
Brian Yasuda
The Air Force Research Labs

Abstract

We describe a new, to our knowledge, scene-based nonuniformity correction algorithm for array detectors. The algorithm relies on the ability to register a sequence of observed frames in the presence of the fixed-pattern noise caused by pixel-to-pixel nonuniformity. In low-to-moderate levels of nonuniformity, sufficiently accurate registration may be possible with standard scene-based registration techniques. If the registration is accurate, and motion exists between the frames, then

groups of independent detectors can be identified that observe the same irradiance (or true scene value). These detector outputs are averaged to generate estimates of the true scene values. With these scene estimates, and the corresponding observed values through a given detector, a curve-fitting procedure is used to estimate the individual detector response parameters. These can then be used to correct for detector nonuniformity. The strength of the algorithm lies in its simplicity and low computational complexity. Experimental results, to illustrate the performance of the algorithm, include the use of visible-range imagery with simulated nonuniformity and infrared imagery with real nonuniformity.

1. Introduction

Focal-plane array (FPA) sensors are widely used in visible-light and infrared imaging systems for a variety of applications. A FPA sensor consists of a two-dimensional mosaic of photodetectors placed in the focal plane of an imaging lens. The wide spectral response and short response time of such arrays, along with their compactness and optical simplicity, give FPA sensors an edge over scanning systems in applications that demand high sensitivity and high frame rates.

The performance of FPA's is known, however, to be affected by the presence of spatial fixed-pattern noise that is superimposed on the true image.[1]-[3] This is particularly true for infrared FPA's. This noise is attributed to the spatial nonuniformity in the photoresponses of the individual detectors in the array. Furthermore, what makes overcoming this problem more challenging is the fact that the spatial nonuniformity drifts slowly in time.[4] This drift is due to changes in the external conditions such as the surrounding temperature, variation in the transistor bias voltage, and the variation in the collected irradiance. In many applications the response of each detector is characterized by a linear model in which the collected irradiance is multiplied by a gain factor and offset by a bias term. The pixel-to-pixel nonuniformity in these parameters is therefore responsible for the fixed-pattern noise.

Numerous nonuniformity correction (NUC) techniques have been developed over the years. For most of these techniques some knowledge of the true irradiance (true scene values) and the corresponding observed detector responses is essential. Different observation models and methods for extracting information about the true scene give rise to the variety of NUC techniques. A standard two-point calibration technique relies on knowledge of the true irradiance and corresponding detector outputs at two distinct levels. With this information the gain and the bias can be computed for each detector and used to compensate for nonuniformity. For infrared sensors two flat-field scenes are typically generated by means of a blackbody radiation source for this purpose.[1],[5],[6] Unfortunately, such calibration generally involves expensive equipment (e.g., blackbody sources, additional electronics, mirrors, and optics) and requires halting the normal operation of the camera for the duration of the calibration. This procedure may also reduce the reliability of the system and increase maintenance costs.

Recently considerable research has been focused on developing NUC techniques that use only the information in the scene being imaged (no calibration targets). The scene-based NUC algorithms generally use an image sequence and rely on motion between frames. Scribner *et al*.[3],[7],[8] developed a least-mean-square-based NUC technique that resembles adaptive temporal high-pass filtering of frames. O'Neil[9],[10] developed a technique that uses a dither scan mechanism that results

in a deterministic pixel motion. Narendra and Foss,[11] and more recently, Harris[12] and Harris and Chiang,[13] developed algorithms based on the assumption that the statistics (mean and variance) of the irradiance are fixed for all pixels. Cain *et al*.[14] considered a Bayesian approach to NUC and developed a maximum-likelihood algorithm that jointly estimates the scene sampled on a high-resolution grid, the detector parameters, and translational motion parameters. A statistical technique that adaptively estimates the gain and the bias using a constant-range assumption was developed recently by Hayat *et al*.[15]

In this paper we consider a method to extract information about the true scene that exploits global motion between frames in a sequence. If reliable motion estimation (registration) is achievable in the presence of the nonuniformity, then the true scene value at a particular location and frame can be traced along a motion trajectory of pixels. This means that all the detectors along this trajectory are exposed to the same true scene value. If the gains and biases of the detectors are assumed to be uncorrelated along the trajectory, then we may obtain a reasonable estimate of the true scene by taking the average of these observed pixel values. This represents a simple motion-compensated temporal average. Furthermore, in a sequence of frames, each detector is potentially exposed to a number of scene values (which can be estimated). Thus the gain and bias of each detector can be estimated with a line-fitting procedure. The observed pixel values and the corresponding estimates of the true scene values form the points used in the line fitting. The procedure may be repeated periodically to account for drift in gain and bias. Although the proposed algorithm may be viewed as heuristic in nature, we believe that it is intuitive and that its strength lies in its simplicity and low computational cost. Furthermore, it appears to offer promising results on the data sets tested.

The remainder of this paper is organized as follows. In Section 2 the proposed NUC algorithm is defined and a statistical error analysis is presented. In Section 3 experimental results are presented. These results illustrate the performance of the algorithm with visible-range images with simulated nonuniformities and forward-looking infrared (FLIR) imagery with real nonuniformities. Finally, some conclusions are presented in Section 4.

2. Nonuniformity Correction

In this section we describe the proposed NUC algorithm in detail and present a statistical analysis. The proposed technique is based on three steps, which are illustrated in Fig. 1. First, registration is performed on a sequence of raw frames. We show in the results section that, unless the levels of nonuniformity are high, a fairly accurate registration can be performed in the case of global motion. The registration algorithm used here is a gradient-based method.[16],[17] Other methods may also be suitable for this application. The next step in the proposed algorithm involves estimating the true scene data with a motion-compensated temporal average. Finally, the observed data and the estimated scene data are used to form an estimate of the nonuniformity parameters. These parameters can then be used to correct future frames with minimal computations. We now describe, in detail, the estimation of the true scene data and the nonuniformity parameters.

A. Estimation of the True Scene

Consider a sequence of desired (true) image frames that are free from the effects of detector nonuniformity. Let us define these data in lexicographical order such that $z_i(j)$ represents the jth pixel

value in the *i*th frame. Let *N* be the number of frames in a given sequence and *P* be the number of pixels per frame.

Here we assume a linear detector response and model the nonuniformity of each detector with a gain and a bias. For the *j*th pixel of the *i*th frame, where $1 \le i \le N$ and $1 \le j \le P$, the observed pixel value is given by (1)

$$x_i(j) = a(j)z_i(j) + b(j),$$

where the variable $a(j)$ represents the gain of the *j*th detector and $b(j)$ is the offset of the detector. These gains and biases are assumed to be constant for each detector over the duration of the *N* frame sequence.

Let us assume that each ideal pixel value in the first frame maps to a particular pixel in all subsequent frames. Thus we neglect border effects and assume that no occlusion or perspective changes occur. This is often reasonable when objects are imaged at a relatively large distance where the motion is the result of small camera pointing angle movement and/or jitter. Furthermore, our mathematical development does not explicitly treat the case of subpixel motion (although the proposed algorithm can be used with subpixel motion). To describe this frame-to-frame pixel mapping or trajectory, let $t_{i,j,k}$ be the spatial index of $z_i(j)$ as it appears in the *k*th frame. This index is determined from the registration step. Thus (2)

$$z_i(j) = z_k\left(t_{i,j,k}\right)$$

for $i = 1, 2, \ldots, N$, $j = 1, 2, \ldots, P$, and $k = 1, 2, \ldots, N$. An example illustrating the use of the notation is shown in Fig. 2.

Here we adopt the assumption that the detector gains and biases are independent and identically distributed from pixel to pixel. We believe that this is reasonable for many applications. In this case let the probability density function of the gain and the bias parameters be denoted $f_a(x)$ and $f_b(x)$, respectively. To achieve relative NUC from pixel to pixel (without calibrated targets, absolute gain and bias values cannot be determined), there is no loss of generality in assuming that the mean of the gain parameters is 1, whereas the mean of the bias terms is 0. If so, the mean of an observed value is the desired scene value, $E\{x_i(j)\} = z_i(j)$. The probability density function of the observed value is given by

(3)

$$f_{x_i(j)}(x) = \frac{1}{z_i(j)} f_a[z_i(j)x] \ * \ f_b(x),$$

where * represents convolution. If the gains and the biases are Gaussian, $x_i(j)$ will also have a Gaussian distribution with mean $z_i(j)$. Furthermore, if the variance of the gains is σ_a^2, and is σ_b^2 for the biases, then the variance of $x_i(j)$ is $\sigma_{xi(j)}^2 = [z_i(j)\sigma_a]^2 + \sigma_b^2$.

If motion is present in the scene, then one has the luxury of making multiple observations of the same scene value through independent detectors. In the case of Gaussian parameters the maximum-likelihood estimate of the desired scene value is given by the sample mean estimate.[18] In particular, this estimate is

(4)

$$\hat{z}_i(j) = \frac{1}{N}\sum_{k=1}^{N} x_k(t_{i,j,k}) = \frac{1}{N}\sum_{k=1}^{N} a(t_{i,j,k}) z_k(t_{i,j,k}) + b(t_{i,j,k}),$$

which reduces to

(5)

$$\hat{z}_i(j) = \frac{1}{N}\sum_{k=1}^{N} a(t_{i,j,k}) z_i(j) + b(t_{i,j,k}),$$

in light of Eq. (2). A convenient way to generate these sample mean estimates in practice is to register and align the temporal frames and then perform a temporal average at each pixel (motion-compensated temporal average). The alignment can be done easily in the case of whole-pixel motion. In the case of subpixel motion, the alignment can be achieved by use of some appropriate interpolation method. The following statistical analysis, however, applies only to the whole-pixel motion case.

Since the desired frames are all related by means of the motion parameters, an estimate for only one frame is needed (e.g., $i = 1$). We can obtain the others by simply applying the motion to the one estimated frame. In particular,

(6)

$$\hat{z}_1(j) = \hat{z}_2(t_{1,j,2}) = \cdots = \hat{z}_N(t_{1,j,N}).$$

For Gaussian nonuniformity parameters these estimates are themselves Gaussian. In general, each estimate has a mean equal to the true scene value, $E\{\hat{z}_i(j)\} = z_i(j)$, and a variance of

(7)

$$\sigma^2_{\hat{z}_i(j)} = \frac{[z_i(j)\sigma_a]^2 + \sigma_b^2}{N}.$$

Thus the estimator variance is signal dependent. The larger $z_i(j)$, the greater the estimator's sensitivity to σ_a.

With an estimate of the desired scene data in hand, we now address the estimation of the nonuniformity parameters. By estimating the nonuniformity parameters themselves, we show that a corrected image can be obtained with lower error variance than that for the estimate in Eq. (5). Furthermore, in most applications, it is useful to know the nonuniformity parameters themselves. For example, knowing the parameters allows one to correct all subsequent frames affected by these

parameters with minimal computation (and without registration). It also provides insight into the nature and level of the system nonuniformity.

B. Estimation of Bias

Let us begin with the case of estimating the bias parameter when there is no gain nonuniformity. In practice this may be an important case, since the bias parameters tend to vary the most and therefore cannot easily be accounted for in an initial manufacturer or laboratory calibration.

In the case of bias-only nonuniformity, the observation model reduces to

(8)

$$x_i(j) = z_i(j) + b(j).$$

In light of this model a reasonable estimate of the bias parameter, $b(j)$, can be obtained from each frame as

(9)

$$\hat{b}_i(j) = x_i(j) - \hat{z}_i(j)$$

for $1 \le i \le N$. Note that in general $\hat{b}_i(j) \ne \hat{b}_k(j)$ for $k \ne i$.

To analyze the estimate in Eq. (9), observe that the estimate of the scene from Eq. (5) can be simplified to

(10)

$$\hat{z}_i(j) = z_i(j) + \frac{1}{N}\sum_{k=1}^{N} b\left(t_{i,j,k}\right).$$

Note that the mean-squared error (MSE) of the estimate is equal to the variance here, since the estimate $\hat{z}_i(j)$ is unbiased. In the case of independent and identically distributed Gaussian biases, we obtain this MSE from Eq. (7) by setting $\sigma_a = 0$, and it is given by σ_b^2/N. With Eqs. (8)–(10) for each frame the bias estimate, $\hat{b}_i(j)$, can be written as

(11)

$$\hat{b}_i(j) = b(j) - \frac{1}{N}\sum_{k=1}^{N} b\left(t_{i,j,k}\right),$$

and the error is therefore

(12)

$$e_i(j) = b(j) - \hat{b}_i(j) = \frac{1}{N}\sum_{k=1}^{N} b\left(t_{i,j,k}\right).$$

Thus the error is zero mean, and the MSE [the variance of $\hat{b}_i(j)$] is $\sigma_{ei(j)}^2 = \sigma_b^2/N$.

In general it is intuitively clear that an improved estimate of $b(j)$ can be obtained by collective use of information from all the frames. For example, we can take the average of the $\hat{b}_i(j)$ over i to obtain the estimator

(13)

$$\hat{b}(j) = \frac{1}{N}\sum_{i=1}^{N} \hat{b}_i(j).$$

With Eqs. (11) and (13) this estimator can be equivalently expressed as

(14)

$$\hat{b}(j) = b(j) - \frac{1}{N^2}\sum_{i=1}^{N}\sum_{k=1}^{N} b\left(t_{i,j,k}\right) .$$

Thus the error associated with $\hat{b}(j)$ is

(15)

$$e(j) = b(j) - \hat{b}(j) = \frac{1}{N^2}\sum_{i=1}^{N}\sum_{k=1}^{N} b\left(t_{i,j,k}\right).$$

Note however that, owing to the nature of the motion trajectories, some of the biases in the double sum are repeated. That is, the sum does not involve N^2 distinct biases, and the redundancy will depend on the specific motion trajectory.

A lower bound on the MSE can be specified when we recognize that the best-case trajectory is the one that results in the least number of redundant terms in Eq. (15). An example of one such trajectory in the case of three frames is illustrated in Fig. 3. The circle, box, and cross represent three true scene values that are observed by the different detectors. Note that the trajectory for the cross is given by $t_{1,10,1} = 10$, $t_{1,10,2} = 11$, and $t_{1,10,3} = 15$. The other trajectories are similar. When the three trajectories are superimposed on one frame (bottom figure), it becomes clear which detectors are involved in the sum in Eq. (15). In particular, one term is present N times and the others are present only once. With this fact, a lower bound on the MSE can be shown to be

(16)

$$\sigma_{e(j)}^2 \geq \left(\frac{2}{N^2} - \frac{1}{N^3}\right)\sigma_b^2.$$

We can also determine an upper bound for the MSE by looking at the worst case. The fewest independent biases exist in the sum when the motion is global and linear. Here $2N - 1$ independent

biases are found in the sum. One bias is included N times, whereas two are included N - 1 times, and two more are seen N - 2 times, etc. Using this observation, the worst-case MSE can be computed as

(17)

$$\sigma_{e(j)}^2 \leq \left(\frac{2}{3N} + \frac{1}{3N^3}\right)\sigma_b^2.$$

The upper and the lower bounds are shown in Fig. 4 as functions of N, where $\sigma_b{}^2 = 1$. Note that the estimate does not improve dramatically after approximately $N = 20$. Note also that the error bounds for the estimate $\hat{b}(j)$, denoted $\sigma_{e(j)}$, are lower than the single frame error $\sigma_{ei\ (j)}$. This clearly demonstrates the benefit of forming an average of $\hat{b}_i(j)$ over i for the final estimate.

Once the biases are estimated, corrected frames may be obtained with

(18)

$$\hat{z}_i^c(j) = x_i(j) - \hat{b}(j).$$

This estimate is unbiased and has an error given by that in Eq. (15). Note that the MSE of this estimate [bounded by relations (16) and (17) when motion exists] is lower than that for the motion-compensated temporal average. The biases can be reestimated periodically to account for slow drift in the parameters.

C. Estimation of Gain and Bias

This subsection describes the estimation of the nonuniformity parameters $a(j)$ and $b(j)$, given the scene estimate from Eq. (5) and the observed data. To begin, we express the estimated scene in terms of the desired (true) value plus an estimator error term,

(19)

$$\hat{z}_i(j) = z_i(j) + \eta_i(j).$$

The estimator error $\eta_i(j)$ is a zero-mean Gaussian random variable with a variance given by Eq. (7). Using (19) in conjunction with our original nonuniformity model in Eq. (1), we obtain

(20)

$$x_i(j) = a(j)\left[\hat{z}_i(j) - \eta_i(j)\right] + b(j) = a(j)\hat{z}_i(j) + b(j) - a(j)\eta_i(j).$$

For notational convenience define $n_i(j) \triangleq -a(j)\eta_i(j)$, which is a zero-mean Gaussian random variable with variance

(21)

$$\sigma_{n_i(j)}^2 = a(j)^2\sigma_{\hat{z}_i(j)^2} = a(j)^2\frac{[z_i(j)\sigma_a]^2 + \sigma_b^2}{N}.$$

Rewriting the expression for $x_i(j)$ gives

(22)

$$x_i(j) = a(j)\hat{z}_i(j) + b(j) + n_i(j).$$

By using multiple frames for each detector, we obtain a set of equations from Eq. (22). Note that the noise term will be signal dependent and will be correlated from frame to frame. This makes an optimum estimate trajectory dependent and difficult to obtain. We believe, however, that a least-squares fit through the observed data and the estimated desired data yields a useful and practical solution. The least-squares solution is that which minimizes the quadratic form

(23)

$$E(\mathbf{a}_j) = |\mathbf{x}_j - Z_j\mathbf{a}_j|^2 = (\mathbf{x}_j - Z_j\mathbf{a}_j)^T(\mathbf{x}_j - Z_j\mathbf{a}_j),$$

where $\mathbf{x}_j = [x_1(j), x_2(j), \ldots, x_N(j)]^T$, $\mathbf{a}_j = [a(j), b(j)]^T$, and

(24)

$$Z_j = \begin{bmatrix} \hat{z}_1(j) & \hat{z}_2(j) & \cdots & \hat{z}_N(j) \\ 1 & 1 & \cdots & 1 \end{bmatrix}^T.$$

Differentiating with respect to the vector quantity $\mathbf{a}_j$ and setting this to zero yields the well-known least-squares result[18]

(25)

$$\hat{\mathbf{a}}_j = \underset{\mathbf{a}_j}{\arg\min}\,(\mathbf{x}_j - Z_j\mathbf{a}_j)T(\mathbf{x}_j - Z_j\mathbf{a}_j) = (Z_j^T Z_j)^{-1} Z_j^T \mathbf{x}_j,$$

where $\hat{\mathbf{a}}_j = [\hat{a}(j), \hat{b}(j)]^T$.

This can be viewed as fitting a straight line between the estimates of the various true scene values and the corresponding outputs for a given detector. Note that, if the scene estimates have no error [i.e., $n_i(j) = 0$, for $1 \le i \le N$], we obtain a set of N consistent equations and the estimate in Eq. (25) would yield the exact solution. However, the scene estimates will invariably have some error in them. Thus it is important for there to be a relatively large range of observed values to get an accurate estimate of the gain and the bias. If the range of observed values is small compared with the error in the scene estimates, a reliable gain and bias estimate may not be possible with this least-squares method. More will be said about this in Subsection 3.B. Finally, with estimates of the gain and the bias in hand, the corrected frames are obtained with

(26)

$$\hat{z}_i^c(j) = \frac{x_i(j) - \hat{b}(j)}{\hat{a}(j)}.$$

3. Experimental Results

In this section a number of experimental results are presented. These include the use of visible-range images with simulated nonuniformities and FLIR video with real nonuniformities. First, however, an analysis of registration accuracy in the presence of nonuniformity is presented.

A. Registration Accuracy with Nonuniformity

Since registration is the key to the proposed algorithm, here we investigate the ability of the selected registration algorithm to operate in the presence of nonuniformity. To do so, a 128 × 128 visible-range 8-bit gray-scale image is first globally shifted according to a known trajectory. The shifted frames are then corrupted with simulated Gaussian gain and bias nonuniformity. A typical corrupted image is shown in Fig. 6(b) below, where the gain standard deviation is 0.1 and the standard deviation of the bias nonuniformity is 10. The images are then registered with an iterative gradient-based algorithm.[16],[17] The mean absolute error between the true and the estimated trajectory is calculated for various levels of nonuniformity. The resulting errors are shown in Fig. 5. Note that the mean absolute error is less than one pixel spacing when σ_a and σ_b are less than approximately 0.3 and 50, respectively. Thus, for light to moderate levels of nonuniformity, such registration may be sufficiently accurate.

If the nonuniformities are too large to obtain good registration initially, it may be necessary to use another NUC technique to begin. For example, the algorithm developed by Hayat *et al*.[15] can be used, since it does not rely on registration. Once the nonuniformity is sufficiently reduced, the proposed method can be used for periodic updates. Such a procedure may offer a computational savings (particularly for the simple bias-only correction). It is also possible to use the proposed method iteratively as a means of coping with large nonuniformities.

B. Nonuniformity Correction with Simulated Data

A sequence of 20 frames of the visible-range data with simulated nonuniformity is used to test the proposed gain and bias estimation algorithm. The first ideal frame with no nonuniformity is shown in Fig. 6(a). This frame with simulated nonuniformity (σ_a = 0.1 and σ_b = 10) is shown in Fig. 6(b). The result of the motion-compensated temporal average is shown in Fig. 6(c). The estimated gains and biases are computed for each pixel and then used to correct the corrupted frames. The corrected first frame is shown in Fig. 6(d). Note that several of the pixels appear to be erroneous (i.e., too dark or light). This is because those detectors were not exposed to a sufficiently wide range of scene values in the 20-frame sequence.

The insufficient range problem is illustrated more clearly in Fig. 7. In these plots the solid lines represent the true detector response curves. Now consider the 20 detector outputs (observed values) for a specific detector over the 20-frame sequence. These values are plotted against the true scene values (known because we simulated the nonuniformity) and are shown as circles. These lie exactly on the detector response curve. The *x*'s represent these same 20 detector outputs plotted against the corresponding estimated scene values. The dashed lines are the least-squares estimated response curves from these data. Figure 7(a) shows an example where the motion resulted in a large range of scene values through the given detector. In this case the algorithm produces an accurate gain and bias estimate. However, for some detectors, the motion does not generate a sufficiently large range of

values. An example of such a case is illustrated in Fig. 7(b). Note that the scene data (and the observed data) are tightly clustered and that the estimated gain and bias are far from the correct values.

For detectors producing a range of values (over the *N* frame sequence) that is below some threshold we recommend one of two approaches. One, those detectors can remain uncorrected for the given image sequence. During future cycles of the process it is likely that such a detector will see a sufficient range in scene values to allow for correction at that time. Alternatively, a bias-only estimate could be performed for those detectors (or all detectors). Such estimates do not require more than one scene value to be observed by a given detector. Using these effective biases can work reasonably well for a limited range of input values, provided that the gains do not vary too much.

The effective bias approach is illustrated in Fig. 8. Figure 8(a) shows four possible detector response curves with varying gains and biases. Figure 8(b) shows the four responses after an effective bias correction is performed so that the detectors respond uniformly at a single point. Near this point, the corrected detectors will respond similarly. The useful range of operation will depend on the variation in the gains. Figure 9 shows the image from Fig. 6(a) corrected with bias-only correction across the entire image.

C. Nonuniformity Correction in Forward-Looking Infrared Video

Here we test the proposed algorithm, using a FLIR system with real nonuniformity. These data have been provided courtesy of the Multi-function Electro-Optics Sensor Branch at the Air Force Research Labs, Wright Patterson Air Force Base Ohio. The FLIR uses a 128 × 128 Amber AE-4128 infrared FPA. The FPA is composed of indium–antimonide (InSb) detectors with a response in the 3–5 μm wavelength band. This system has square detectors of size $a = b = 0.040$ mm. The imager is equipped with 100-mm $f/3$ optics. A sequence of approximately 3000 frames was acquired by manual panning of the imager from a tower causing a global shift in the frames. The acquisition frame rate is approximately 30 frames/s. A typical frame with no NUC is shown in Fig. 10(a). This frame shows a road crossing the field of view with a variety of trailers and vehicles in the top portion of the image.

A set of 30 frames is registered, and a motion-compensated temporal average is computed [Fig. 10(b)]. Subpixel registration was performed, and the alignment was done with bilinear interpolation. The effective bias terms are estimated and are shown in Fig. 10(c). The first frame, corrected with these biases, is shown in Fig. 10(d). With the exception of some border effects (which occur because all frames do not share the exact same field of view), the results appear to be promising, on the basis of subject evaluation. The processing was performed with MATLAB software on a Sun Ultra10 computer. In our implementation (not fully optimized) the estimation of the biases and subsequent correction of the 30-frame sequence takes approximately 15 s.

A frame collected approximately 10 s apart from the 30-frame sequence was also corrected with these estimated effective biases. Here we wanted to evaluate how well one set of effective biases could perform on new data, not used in the bias estimation process. The corrupted frame is shown in Fig. 11(a), and the corrected frame is shown in Fig. 11(b). This image also appears to show significant improvement. Thus it appears that no significant parameter drift has taken place in this short time. Furthermore, the image demonstrates that parameters estimated from one set of frames can be useful in correcting subsequent frames, which may contain different scenes.

4. Conclusions

We have presented a scene-based NUC algorithm that exploits motion in an image sequence. We believe that the strength of the proposed algorithm lies in its simplicity and low computational complexity. The key requirement for the algorithm is accurate motion estimation. In the experimental results presented we have shown that, when relatively small to moderate levels of nonuniformity exist, it may be possible to perform accurate global registration. However, if severe nonuniformity is present, scene-based motion estimation may not be reliable.[19] With proper registration one can identify a trajectory where a given scene value is observed through multiple detectors. An average along this trajectory yields an estimate of the scene. The scene estimate, along with the corresponding observed data, are then used to form an estimate of the detector nonuniformity parameters.

We have observed that the proposed least-squares gain and bias estimation procedure is sensitive to the range of scene values observed by a given detector. The bias-only estimation procedure, however, does not require more than one scene value to be observed by a detector. In this way the effective bias estimation procedure is more robust. However, if the actual gains do vary, the effective bias correction can make the detectors respond uniformly only at one specific irradiance level. When operating near this level, one can expect good NUC results with effective bias correction.

The authors thank the members of the Multi-function Electro-Optics Sensor Branch at Air Force Research Labs, Wright Patterson Air Force Base, for providing the infrared imagery used here and for the helpful discussions that provided insight into the nonuniformity problem. This research was supported in part by the National Science Foundation (Career Program MIP-9733308).

Figures

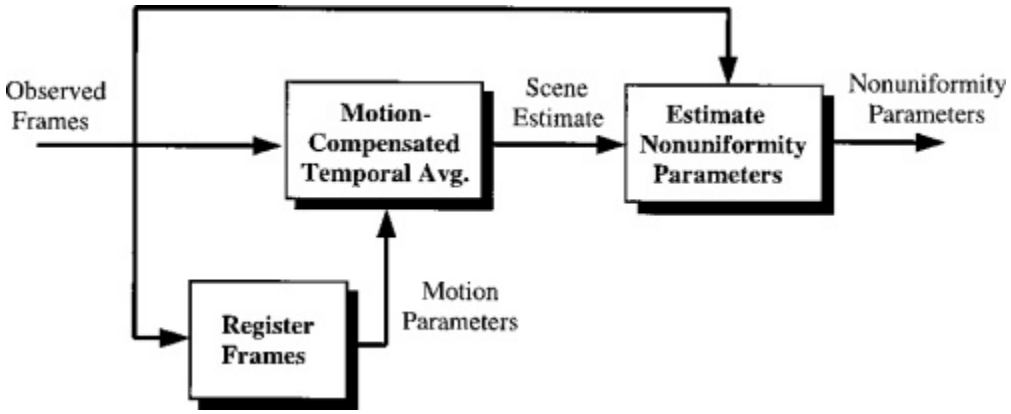

Fig. 1 Block diagram of proposed NUC algorithm.

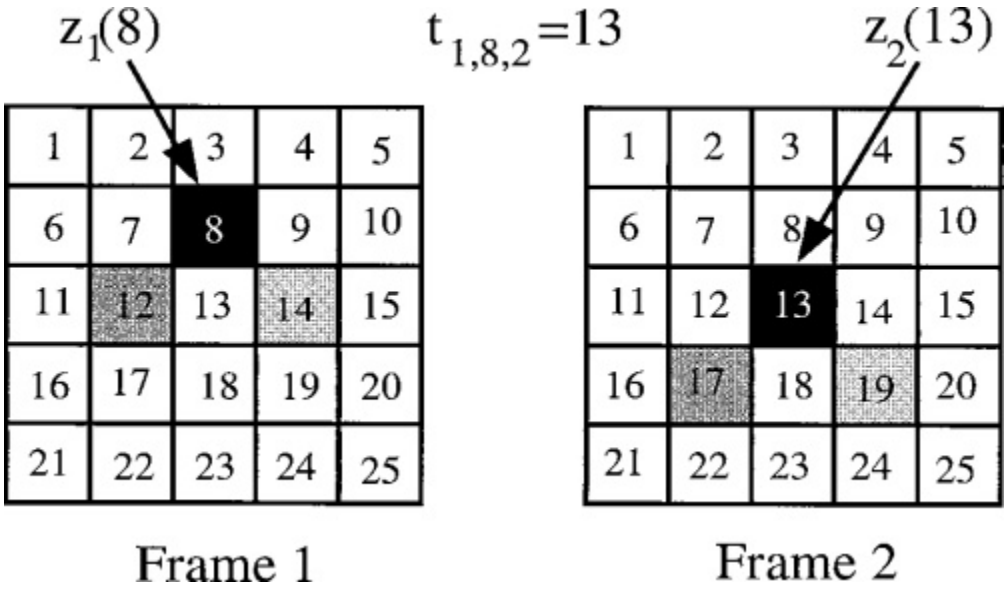

Fig. 2 Two frames showing an example of a motion trajectory. The shaded blocks represent true scene values that move from frame one to frame two. Note that $z_2(13) = z_1(8)$.

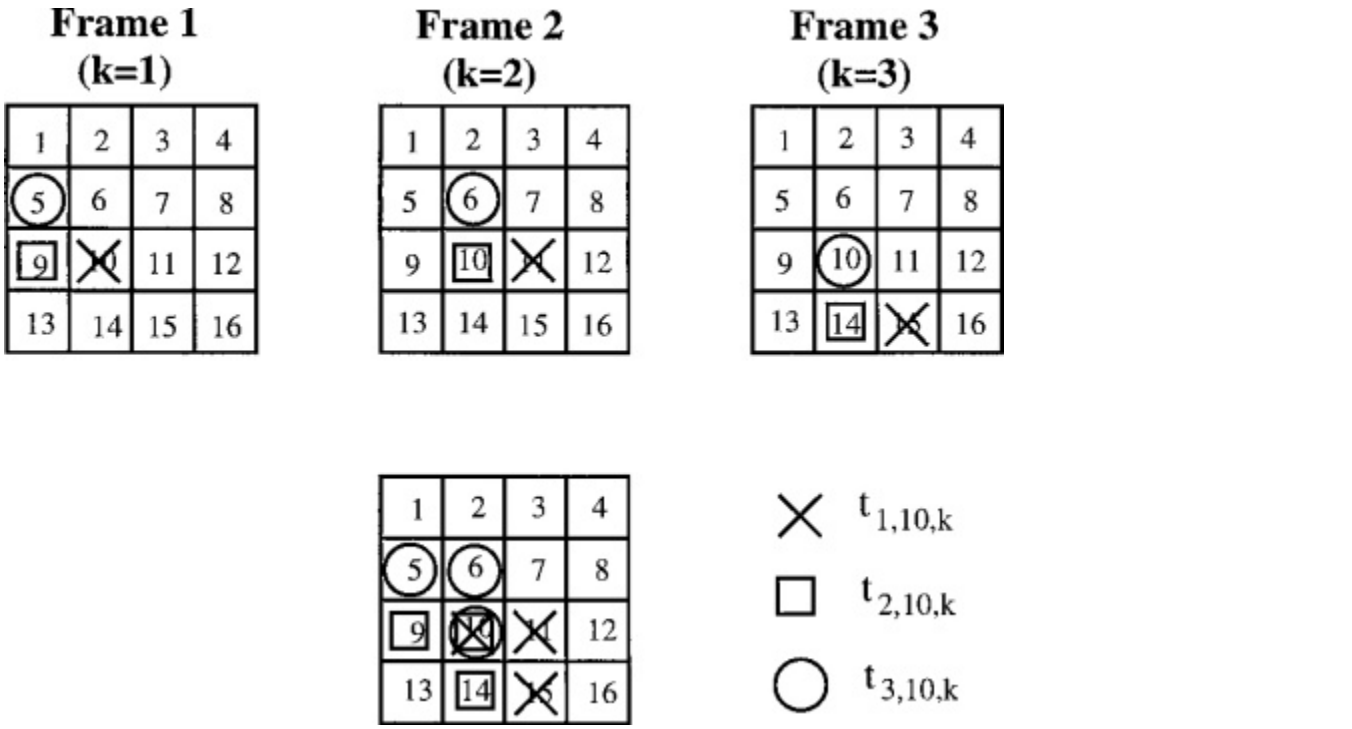

Fig. 3 Example of a three-frame trajectory for the best case. The cross, circle, and square represent different signal values. The bottom figure shows which signal levels are seen by which detectors during

the course of the entire trajectory

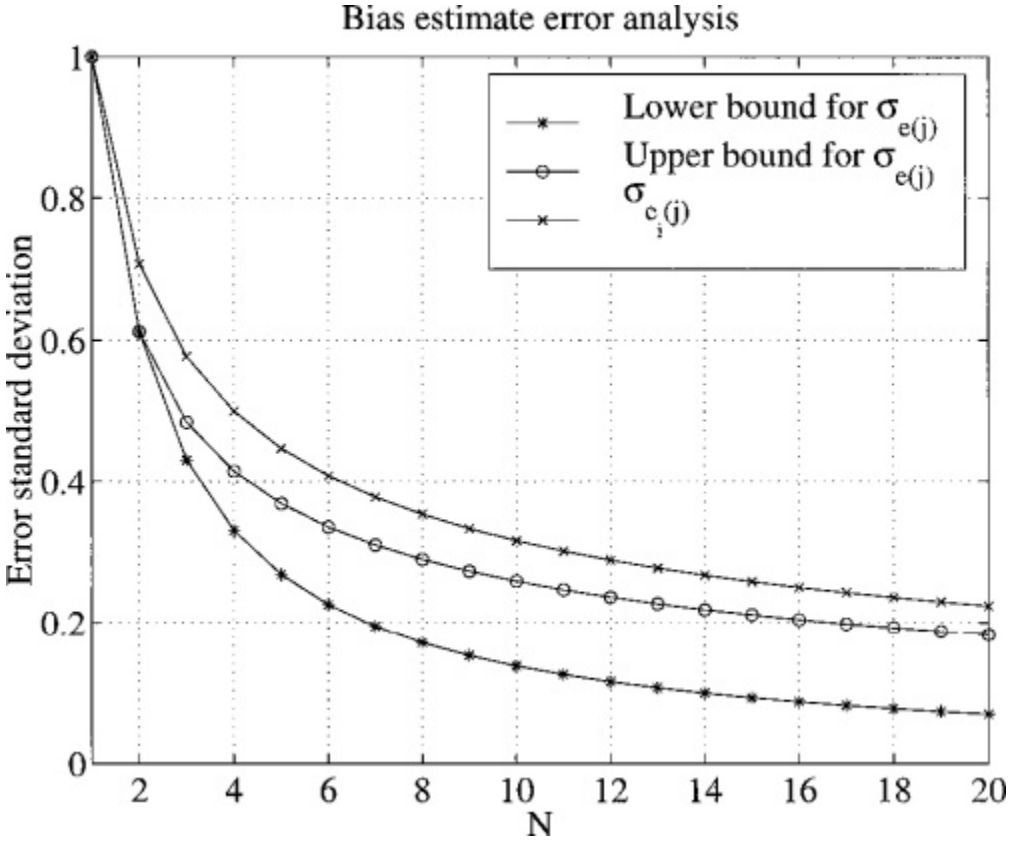

Fig. 4 Standard deviation bounds for the bias estimate error where $\sigma_b^2 = 1$.

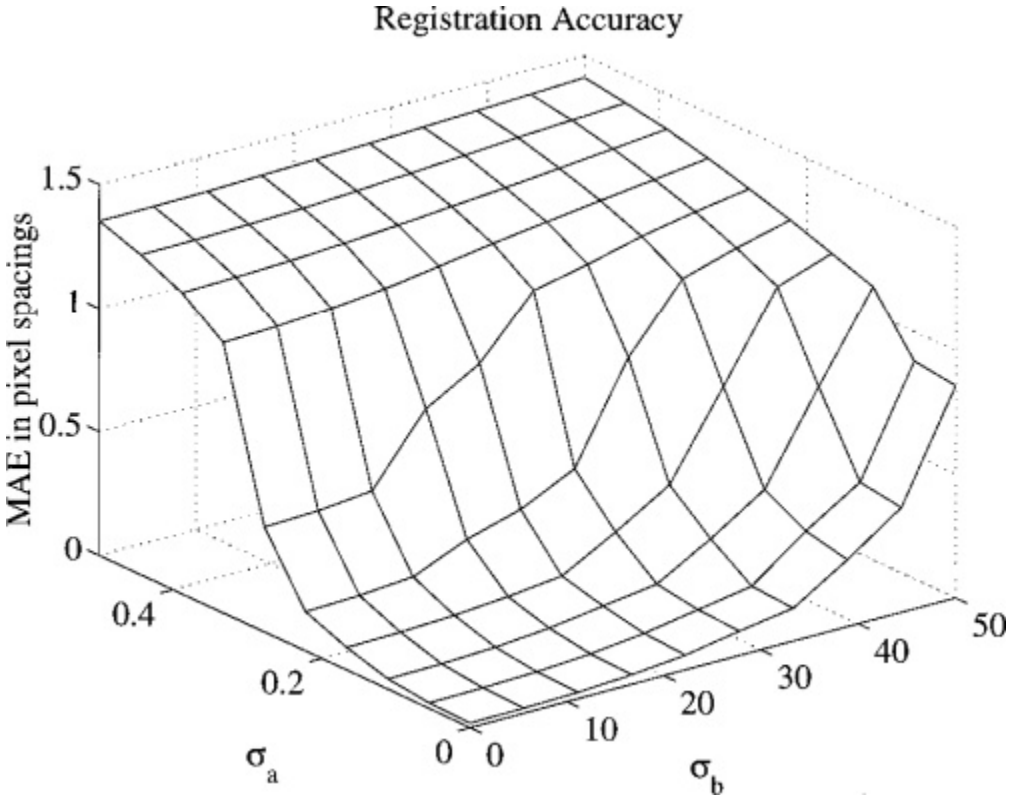

Fig. 5 Registration accuracy with various levels of gain and bias nonuniformity. MAE, mean absolute error.

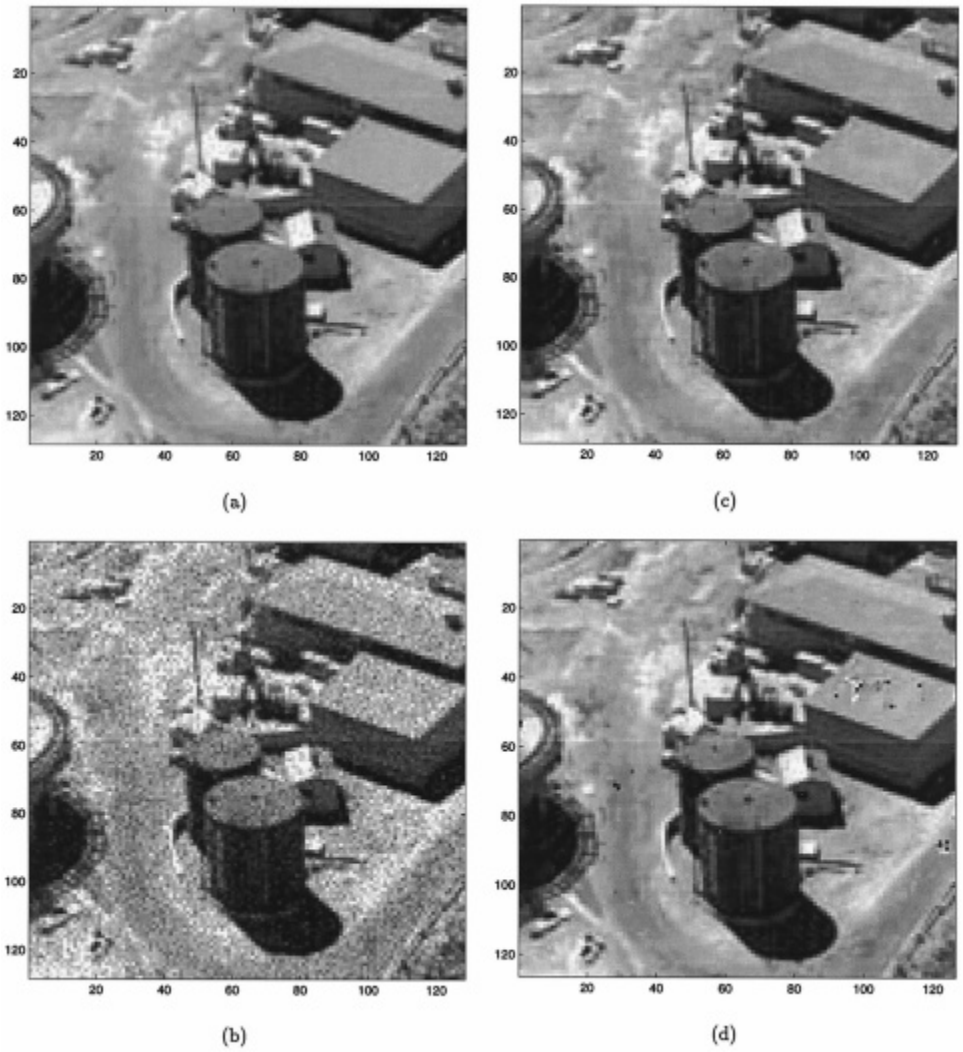

Fig. 6 (a) True frame 1, (b) frame 1 with simulated nonuniformity, (c) motion-compensated temporal average, (d) corrected image with the least-squares parameters.

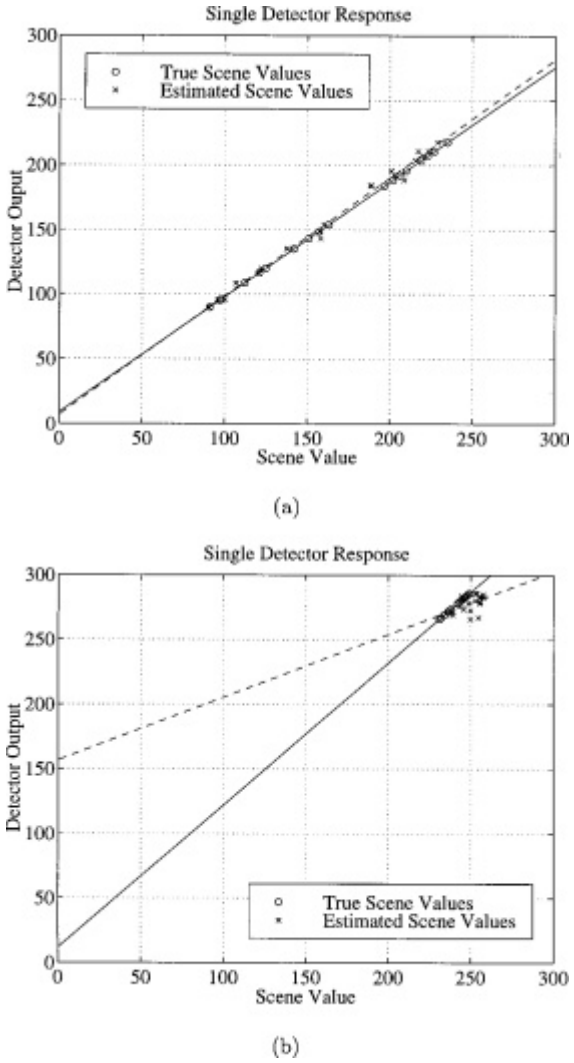

Fig. 7 True detector response curves (solid lines) and estimated responses (dashed lines) when observed data has (a) good range (b) poor range. The detector outputs are plotted versus the true scene values and the estimated scene values.

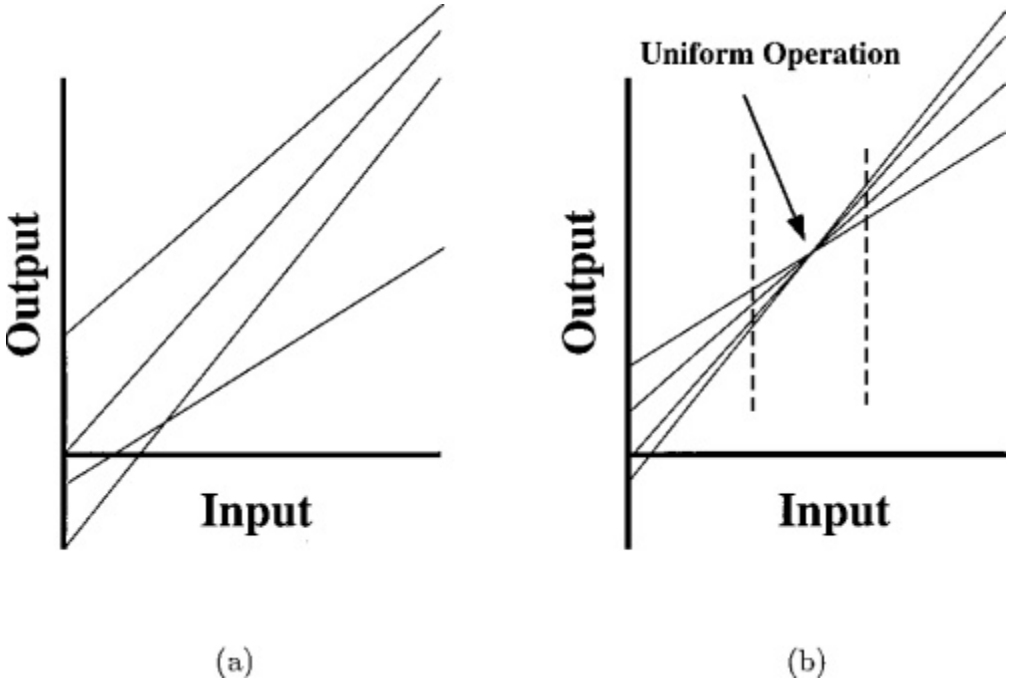

Fig. 8 Illustration of the process of effective bias correction. (a) Raw detector responses, (b) responses after effective bias correction.

Fig. 9 Image with effective bias correction.

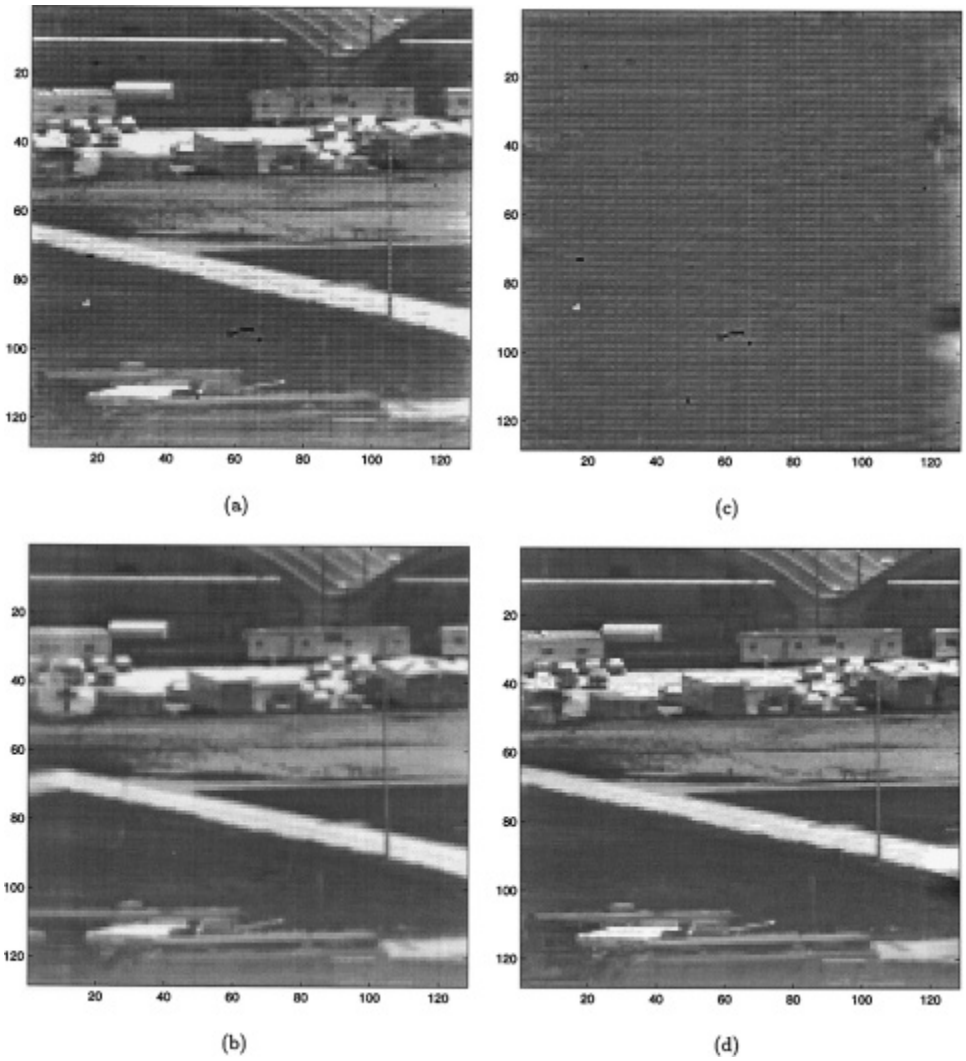

Fig. 10 (a) Original FLIR image with nonuniformity, (b) motion-compensated temporal average, (c) estimated biases for each pixel, (d) corrected image.

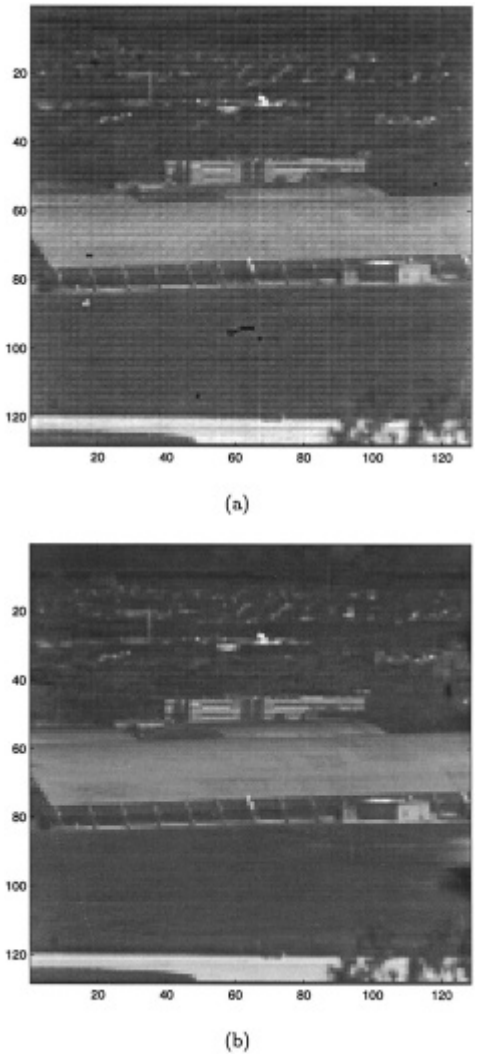

Fig. 11 (a) New FLIR image with nonuniformity (b), corrected image with biases calculated from previous data.

References

1. A. F. Milton, F. R. Barone, and M. R. Kruer, "Influence of nonuniformity on infrared focal plane array performance," Opt. Eng. **24**, 855–862 (1985). [CrossRef]

2. G. C. Holst, *CCD Arrays, Cameras, and Displays* (SPIE Optical Engineering Press, Bellingham, Wash., 1996).

3. D. A. Scribner, K. A. Sarkay, J. T. Caulfield, M. R. Kruer, G. Katz, and C. J. Gridley, "Nonuniformity correction for staring IR focal plane arrays using scene-based techniques," in *Infrared Detectors and Focal Plane Arrays*, E. L. Dereniak and R. E. Sampson, eds., Proc. SPIE 1308, 224–233 (1990).

4. D. A. Scribner, M. R. Kruer, and J. C. Gridley, "Physical limitations to nonuniformity correction in focal plane arrays," in *Technologies for Optoelectronics*, J. M. Bulabois and R. F. Potter, eds., Proc. SPIE 869, 185–201 (1987).

5. D. L. Perry and E. L. Dereniak, "Linear theory of nonuniformity correction in infrared staring sensors," Opt. Eng. **32**, 1853–1859 (1993). [CrossRef]

6. M. Schulz and L. Caldwell, "Nonuniformity correction and correctability of infrared focal plane arrays," Inf. Phys. Technol. **36**, 763–777 (1995). [CrossRef]

7. D. A. Scribner, K. A. Sarkady, M. R. Kruer, J. T. Caulfield, J. D. Hunt, M. Colbert, and M. Descour, "Adaptive retina-like preprocessing for imaging detector arrays," in *Proceedings of the IEEE International Conference on Neural Networks* (Institute of Electrical and Electronics Engineers, New York, 1993), pp. 1955–1960. [CrossRef]

8. D. Scribner, K. Sarkady, M. Kruer, J. Caulfield, J. Hunt, M. Colbert, and M. Descour, "Adaptive nonuniformity correction for infrared focal plane arrays using neural networks," in *Infrared Sensors: Detectors, Electronics, and Signal Processing*, T. S. Jayadev, ed., Proc. SPIE 1541, 100–110 (1991).

9. W. F. O'Neil, "Dithered scan detector compensation," in *Proceedings of the 1993 Meeting of the Infrared Information Symposium (IRIS) Specialty Group on Passive Sensors* (Infrared Information Analysis Center, Ann Arbor, Mich., 1993).

10. W. F. O'Neil, "Experimental verification of dithered scan non-uniformity correction," in *Proceedings of the 1996 Meeting of the Infrared Information Symposium (IRIS) Specialty Group on Passive Sensors* (Infrared Information Analysis Center, Ann Arbor, Mich., 1997), Vol. 1, pp. 329–339.

11. P. M. Narendra and N. A. Foss, "Shutterless fixed pattern noise correction for infrared imaging arrays," in *Technical Issues in Focal Plane Development*W. S. Chan and E. Krikorian, eds., Proc. SPIE 282, 44–51 (1981). [CrossRef]

12. J. G. Harris, "Continuous-time calibration of VLSI sensors for gain and offset variations," in *International Symposium on Aerospace and Dual-Use Photonics, Smart Focal Plane Arrays and Focal Plane Array Testing*, M. Wigdor and M. A. Massie, eds. Proc. SPIE 2474, 23–33 (1995). [CrossRef]

13. J. G. Harris and Y.-M. Chiang, "Nonuniformity correction using constant average statistics constraint: analog and digital implementations," in *Infrared Technology and Applications XXIII*, B. F. Anderson and M. Strojnik, eds. Proc. SPIE 3061, 895–905 (1997). [CrossRef]

14. S. Cain, E. Armstrong, and B. Yasuda, "Joint estimation of image, shifts, and non-uniformities from infrared images," in *Proceedings of the 1997 Meeting of the Infrared Information Symposium (IRIS) Specialty Group on Passive Sensors* (Infrared Information Analysis Center, Ann Arbor, Mich., 1997), Vol. 1, pp. 121–132.

15. M. M. Hayat, S. N. Torres, E. Armstrong, S. C. Cain, and B. Yasuda, "Statistical algorithm for nonuniformity correction in focal-plane arrays," Appl. Opt. **38**, 772–780 (1999). [CrossRef]

16. M. Irani and S. Peleg, "Improving resolution by image registration," CVGIP: Graph. Models Image Process. **53**, 231–239 (1991). [CrossRef]

17. R. C. Hardie, K. J. Barnard, J. G. Bognar, E. E. Armstrong, and E. A. Watson, "High resolution image reconstruction from a sequence of rotated and translated frames and its application to an infrared imaging system," Opt. Eng. **37**, 247–260 (1998). [CrossRef]

18. C. W. Therrien, *Discrete Random Signals and Statistical Signal Processing* (Prentice Hall, Englewood Cliffs, N.J., 1992).

19. E. E. Armstrong, M. M. Hayat, R. C. Hardie, S. Torres, B. Yasuda, "The advantage of non-uniformity correction pre-processing on infrared image registration," in *Applications of Digital Image Processing XXII*, A. G. Tescher, and Lockheed Martin Mission Systems, eds., Proc. SPIE 3808, 156–161 (1999).